The Impact of CFO on OFDM based Physical-layer Network Coding with QPSK Modulation

Ling Fu Xie
Faculty of EECS
Ningbo University
Ningbo, China
xiel0002@ntu.edu.sg

Ivan Wang-Hei Ho and Zhenhui Situ
Dept. of Electronic and Information Engineering
The Hong Kong Polytechnic University
Hong Kong, China
ivanwh.ho@polyu.edu.hk, z.situ@connect.polyu.hk

Peiya Li
College of Cyber Security
Jinan University
Guangzhou, China
lpy0303@jnu.edu.cn

***Abstract*—This paper studies Physical-layer Network Coding (PNC) in a two-way relay channel (TWRC) operated based on OFDM and QPSK modulation but with the presence of carrier frequency offset (CFO). CFO, induced by node motion and/or oscillator mismatch, causes inter-carrier interference (ICI) that impairs received signals in PNC. Our ultimate goal is to empower the relay in TWRC to decode network-coded information of the end users at a low bit error rate (BER) under CFO, as it is impossible to eliminate the CFO of both end users. For that, we first put forth two signal detection and channel decoding schemes at the relay in PNC. For signal detection, both schemes exploit the signal structure introduced by ICI, but they aim for different output, thus differing in the subsequent channel decoding. We then consider CFO compensation that adjusts the CFO values of the end nodes simultaneously and find that an optimal choice is to yield opposite CFO values in PNC. Particularly, we reveal that pilot insertion could play an important role against the CFO effect, indicating that we may trade more pilots for not just a better channel estimation but also a lower BER at the relay in PNC. With our proposed measures, we conduct simulation using repeat-accumulate (RA) codes and QPSK modulation to show that PNC can achieve a BER at the relay comparable to that of point-to-point transmissions for low to medium CFO levels.**

***Index Terms*—OFDM, physical-layer network coding, carrier frequency offset, pilot insertion**

I. Introduction

Non-orthogonal multiple access (NOMA) has received enormous attention from research communities in recent years and is regarded as a candidate solution for the upcoming fifth-generation (5G) cellular networks [1]. This is because NOMA is a performance booster that allows network resources (e.g., frequency spectrum) to be accessed by multiple users simultaneously. Physical-layer Network Coding (PNC) is such a technique that combines network coding and has the potential to double network throughput [2]: In a Two-Way Relay Channel (TWRC) shown in Fig. 1, PNC decreases four times slots needed in traditional point-to-point transmission to *two* when the two end nodes A and B wish to exchange a packet to each other via relay R. Specifically, in time slot 1, nodes A and B use the same frequency band to simultaneously transmit their packets X_A and X_B to relay R, and in time slot 2, relay R, from the received signal, performs XOR decoding, i.e., deduces the network-coded packet $X_R = X_A \oplus X_B$ using XOR, and broadcasts it to nodes A and B. Packet X_R serves both nodes A and B as they can perform $X_R \oplus X_A = X_B$ and $X_R \oplus X_B = X_A$ to obtain their desired packets, respectively.

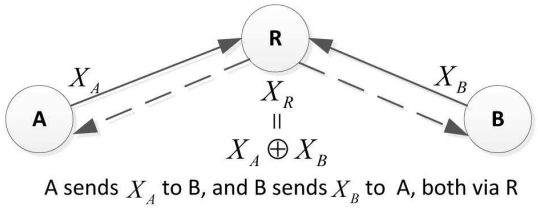

Fig. 1. PNC in a two-way relay channel.

The application of PNC to Orthogonal Frequency Division Multiplexing (OFDM) systems is a focus in PNC studies [3]–[6]. First, OFDM systems nowadays have been gaining popularity for network deployment, e.g., IEEE 802.11/a/g/p protocols, 4G LTE, and 5G cellular networks all have standardized the use of OFDM in the PHY layer. Second, more importantly, PNC suffers from inter-symbol interference (ISI) caused by symbol misalignment of the end nodes [7], [8], but an ISI-free PNC can be easily realized in OFDM systems with adequately long cyclic prefix (CP) [9].

Nonetheless, OFDM based PNC is vulnerable to carrier frequency offset (CFO). CFO can be induced by node motion and/or local oscillator (LO) mismatch between transmitters and receivers. CFO can be estimated and eliminated for a point-to-point link at its receiver [9], whereas this is not the case in PNC at relay R, as relay R generally faces two different CFO values from nodes A and B. CFO in PNC results in not only the inter-carrier interference (ICI) between the subcarriers of nodes A and B, but also a relative phase offset between the received constellations of nodes A and B. Both will cause performance loss in PNC [7], especially for high-order modulations including QPSK [10].

This paper is an attempt to effectively mitigate the adverse effect of CFO on OFDM based PNC in TWRC with QPSK modulation. To this end, we study measures that can be

This work was supported in part by the General Research Fund (Project No. 15201118) established under the University Grant Committee (UGC) of the Hong Kong Special Administrative Region (HKSAR), China; and by The Hong Kong Polytechnic University (Projects G-YBK6, G-YBR2, G-YBXJ). The work of L. F. Xie was supported by the National Natural Science Foundation of China (NSFC) under Project 61601254.

adopted at the end nodes and the relay in TWRC. Specifically, our contributions in this paper are summarized as follows:

- First, we propose two signal detection and channel decoding schemes at relay R in PNC. A repeat-accumulate (RA) channel code is assumed in our study. Both schemes make use of the signal structure introduced by ICI for signal detection, but they diverge from the detection output and then differ in the subsequent channel decoding.
- Second, we study CFO compensation at relay R that adjusts the CFO values of nodes A and B simultaneously and find that an optimal choice is to yield opposite CFO values for QPSK modulation. In fact, this optimal CFO compensation also applies to BPSK modulation, as previously studied in [6].
- Third, we study the pilot insertion at the transmitters A and B and reveal that this could play an important role against the CFO effect in PNC. This may justify the use of more pilots in PNC, as it brings about not just a better channel estimation but also a lower BER at relay R.
- Fourth, we demonstrate by simulation that PNC, with the proposed measures, can achieve a BER at relay R comparable to that of traditional point-to-point transmission for low to medium CFO levels.

II. Related Work

A relative phase offset between the received constellations of the end nodes is a critical issue in PNC studies. It generally degrades the XOR decoding performance in both single-carrier based and OFDM based PNC [4], [10], [11]. For PNC with QPSK modulation, a remedy was introduced in [10] to design different network coding schemes for different relative phase offsets at relay R. However, our study will point out that when CFO comes to play, using any specific network coding scheme suggested by [10] does not make difference in general.

Another critical issue in PNC studies is the symbol offset between the end nodes. When the signals from the end nodes are received not aligned, inter-symbol interference (ISI) usually occurs at relay R and performance loss can also be observed [7], [12]. Fortunately, ISI can be avoided easily for OFDM based PNC using a cyclic prefix (CP) longer than the delay spread of the PNC system [9]. This paper takes advantage of OFDM with an adequately long CP and assumes symbols of the end nodes are aligned in the frequency domain.

OFDM based PNC, however, is confronted with the CFO/ICI problem, because it is not possible to eliminate both CFO of the end nodes, as mentioned earlier. There are some efforts towards attacking this CFO/ICI problem [4], [5], [13], of which most dealt with signal detection and/or channel decoding at relay R. In this paper, we do not only consider effective signal detection and channel decoding schemes in channel-coded PNC, but also study other approaches to further reduce the adverse effect of CFO: One attempt is to seek an optimal CFO compensation at relay R for QPSK modulation (although an optimal compensation was pointed out in [6] for BPSK modulation), and the other attempt is to study the effect of pilot insertion at the transmitters A and B.

Channel estimation is also central to PNC. [8], [16] studied joint channel estimation and decoding for single-carrier PNC, and [3], [9] dealt with the channel and CFO estimation in OFDM based PNC. This paper assumes perfect knowledge of the channel and CFO from the end nodes at relay R.

III. System Model

This section presents the system model of PNC in a TWRC operated based on OFDM and QPSK modulation but with the presence of carrier frequency offset (CFO).

We assume the packets to be transmitted by nodes A and B are bit sequences of equal length, denoted by $X_i = \{x_i[m]\}_{m=0}^{M-1}$, for $i \in \{A, B\}$. Then, X_i passes through a linear channel encoder $\boldsymbol{C}(\cdot)$ of rate $\frac{M}{N}$, yielding $U_i = \boldsymbol{C}(X_i) = \{u_i[n]\}_{n=0}^{N-1}$. This paper uses repeat-accumulate (RA) codes [12], [17]; other channel codes like turbo codes can also be used in our study. With QPSK modulation, U_i is mapped to symbols $S_i = \{s_i[n]\}_{n=0}^{\frac{N-2}{2}}$ using the rule $s_i[n] = \frac{\sqrt{2}}{2}\{(1-2u_i[2n]) + (1-2u_i[2n+1])j\}$. Let K be the number of subcarriers in OFDM, and assume $\frac{N}{2}$, the length of S_i, is a multiple of K for simplicity. Thus, S_i is divided into $L = \frac{N}{2K}$ groups, $S_{i,l} = \{s_i[lK], ..., s_i[(l+1)K-1]\}$, $0 \le l < L = \frac{N}{2K}$, to form L OFDM symbols. Let us focus on the time-domain samples of one OFDM symbol $l = 0$:

$$v_i[m] = \frac{1}{\sqrt{K}} \sum_{k=0}^{K-1} s_i[k] e^{j2\pi km/K}, -N_g \le m < K, \quad (1)$$

where $v_i[m]$ is the m-th sample from node i and N_g is the number of CP samples. In the following, we consider both flat and frequency-selective fading channels in TWRC together with a power control scheme.

A. The Flat Fading Channel Case

For a flat fading channel from node i to relay R, the multipath channel gain has only one tap, denoted by $h_i[m]$ at the m-th sample time. We assume block fading for $h_i[m]$, that is, it keeps constant over one packet transmission period. Thus, the m-th received sample at relay R in PNC is

$$v_R[m] = h_A v_A[m] + h_B v_B[m] + w[m], -N_g \le m < K, \quad (2)$$

where h_i is the channel gain and $w[m]$ is circularly symmetric Gaussian noise with mean 0 and variance σ^2.

Relative motion and/or LO mismatch between relay R and the end nodes will induce CFO. First, due to LO instability, the frequency generated by a LO may deviate from a desired one, which results in a CFO between relay R and node i. This CFO is given by $f_{o,i} - f_{o,R}$, with $f_{o,i}$ ($f_{o,R}$) being the carrier frequency of node i (relay R). Second, relative motion between relay R and node i induces Doppler shift $f_{d,i} = \frac{m_i}{c} f_{o,i}$, where m_i and c are the speeds of motion and waves, respectively. We consider a narrow-band TWRC where $f_{d,i}$ applies to all frequency components of a signal and so does the aggregate CFO $f_{\delta_i} = f_{d,i} + f_{o,i} - f_{o,R}$ [19]. Third, it is not the absolute CFO f_{δ_i} but the normalized one $\delta_i = f_{\delta_i}/\Delta_f$ (Δ_f is the subcarrier spacing) that is critical to an OFDM system [20]. Our study assumes $-0.5 \le \delta_i \le 0.5$; this

is usually an enlarged range for modern networks using stable LO and electromagnetic waves [4]. With CFO δ_i involved, the received sample $v_R[m]$ becomes

$$v_R[m] = h_A e^{j2\pi\delta_A m/K} v_A[m] + h_B e^{j2\pi\delta_B m/K} v_B[m] + w[m]. \tag{3}$$

Taking DFT on the samples $\{v_R[m]\}_{m=0}^{K-1}$ yields the m-th received frequency-domain sample

$$\begin{aligned} s_R[m] &= \frac{1}{K} \sum_{i\in\{A,B\}} \sum_l h_i c_i[l] s_i[m-l] + \tilde{w}[m] \\ &= \frac{1}{K} \sum_{i\in\{A,B\}} \left[\underbrace{h_i c_i[0] s_i[m]}_{\text{desired signal}} + \underbrace{\sum_{l\neq 0} h_i c_i[l] s_i[m-l]}_{\text{ICI}} \right] + \tilde{w}[m], \end{aligned} \tag{4}$$

where $\tilde{w}[m]$ has mean 0 and variance σ^2 and $c_i[l]$ is given by

$$c_i[l] = \frac{1 - e^{j2\pi(\delta_i - l)}}{1 - e^{j2\pi(\delta_i - l)/K}}, m - K + 1 \le l \le m. \tag{5}$$

We see from (4) and (5) that for $\delta_i \neq 0$ ICI arises at any subcarrier m.

B. The Frequency-Selective Channel Case

For a frequency-selective channel from node i to relay R, the multipath channel gain has multiple taps and is represented by $\{h_i[n]\}_{n=0}^{L_c-1}$ assuming block fading over a packet transmission period. For a long CP, $N_g > L_c$ holds. For $0 \le m < K$, the received m-th time-domain sample at relay R in PNC is

$$\begin{aligned} v_R[m] &= \sum_{i\in\{A,B\}} e^{j\frac{2\pi\delta_i m}{K}} v_i[m] \otimes h_i[m] + w[m] \\ &= \sum_{i\in\{A,B\}} e^{j\frac{2\pi\delta_i m}{K}} \sum\nolimits_{k=0}^{L_c-1} h_i[k] v_i[m-k]_K + w[m], \end{aligned} \tag{6}$$

where $\otimes$ denotes circular convolution and $[m-k]_K$ denotes $[m-k]$ modulo K.

Taking DFT on $\{v_R[m]\}_{n=0}^{K-1}$ yields

$$\begin{aligned} & s_R[m] \\ &= \frac{1}{K} \sum_{i\in\{A,B\}} \left[\underbrace{c_i[0]\tilde{h}_i[m] s_i[m]}_{\text{desired signal}} + \underbrace{\sum_{l\neq 0} c_i[l]\tilde{h}_i[m-l] s_i[m-l]}_{\text{ICI}} \right] \\ &\quad + \tilde{w}[m], \end{aligned} \tag{7}$$

where $\{\tilde{h}_i[m]\}_{m=0}^{K-1}$ is the K-point DFT of $\{h_i[m]\}$.

C. Power Control Scheme

We consider the following power control scheme at node i: given a power budget P_i at node i, the received powers for all subcarriers at relay R are the same. This ensures that no particular subcarrier will become a bottleneck in PNC. With the channel gains feed-backed to node i, node i amplifies the signal of the m-th subcarrier as follows: $\frac{F_i}{\|\tilde{h}_i[m]\|} \cdot s_i[m]$, where F_i is given by

$$F_i = \sqrt{\frac{P_i}{\sum_{k=0}^{K} \frac{1}{\|\tilde{h}_i[k]\|^2}}}. \tag{8}$$

Note that $\tilde{h}_i[k]$ in (8) reduces to h_i in flat fading channel. Compared with [18], our scheme does not precode the phase (denoted by $\varphi_{i,m}$ below) of $\tilde{h}_i[m]$ and is thus less demanding. With the power control, (7) becomes

$$s_R[m] = \frac{1}{K} \sum_i \sum_l e^{j\varphi_{i,m}} c_i[l] F_i s_i[m-l] + \tilde{w}_m. \tag{9}$$

IV. XOR Decoding in PNC

A. Signal Detection and Channel Decoding in PNC

This subsection presents the XOR decoding of $X_R = X_A \oplus X_B$ at relay R from the KL received samples of L OFDM symbols (see (9) for the 1-st OFDM symbol). This can be done in two ways: one is to obtain the *a posteriori* probabilities (APPs) of the bit vectors $\{(u_A[2n], u_A[2n+1], u_B[2n], u_B[2n+1])\}_{n=0}^{\frac{N-2}{2}}$ and then channel-decode $\{x_A[m] \oplus x_B[m]\}_{m=0}^{M-1}$; and the other is to obtain the APPs of $\{u_A[n] \oplus u_B[n]\}_{n=0}^{N-1}$ and then channel-decode $\{x_A[m] \oplus x_B[m]\}_{m=0}^{M-1}$. They correspond to the two signal detection and decoding schemes below, namely, the Joint Channel-decoding and Network Coding (Jt-CNC) and the XOR and Channel-Decoding (XOR-CD). Here, we stress that apart from the network coding scheme $X_R = X_A \oplus X_B$, other scheme(s) exists [10], as will be discussed in this section.

Signal detection of Jt-CNC: This uses the received samples of each individual OFDM symbol to compute the APPs of every involved $(u_A^{2n,2n+1}, u_B^{2n,2n+1}) = (u_A[2n], u_A[2n+1], u_B[2n], u_B[2n+1])$. Following [4], for the ICI terms in (9), we only consider the dominating interfering subcarrier from node i: it is the $(m-1)$-th subcarrier for $\delta_i > 0$ and the $(m+1)$-th subcarrier otherwise. Thus, we have four cases to compute the APP above: (1) $\delta_A > 0$ and $\delta_B > 0$, (2) $\delta_A > 0$ and $\delta_B \le 0$, (3) $\delta_A \le 0$ and $\delta_B > 0$, and (4) $\delta_A \le 0$ and $\delta_B \le 0$. Here, we focus on case (1); the others are similar. We create a factor graph in the lower part of Fig. 2 to capture how the variables S_A and S_B are involved to generate the KL received samples under CFO. The factor graph includes

- the variable/square nodes: the n-th variable node is given by $(s_A^{n,n-1}, s_B^{n,n-1}) = (s_A[n], s_A[n-1], s_B[n], s_B[n-1]), 0 \le n < \frac{N}{2}$, where $n-1$ indicates the dominating interfering subcarrier number.
- the red check/circle nodes: this ensures that the two variable nodes connected to a common red check node should assign the same values for their common variables.
- the white check/circle nodes: each check node here provides its connected variable node with the APPs of $(s_A^{n,n-1}, s_B^{n,n-1})$ based on the local observed sample. These APPs are encapsulated into a message denoted by

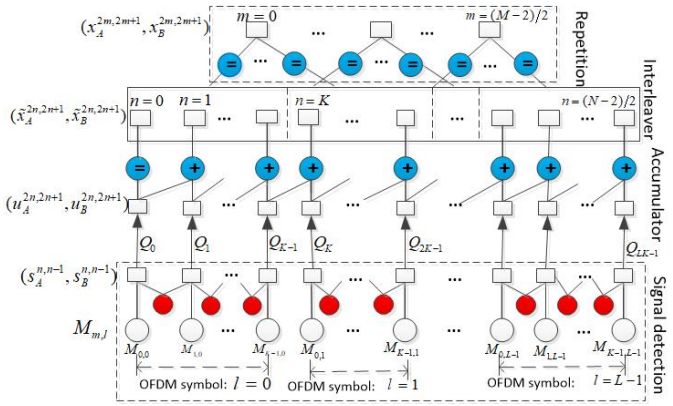

Fig. 2. A factor graph of Jt-CNC.

$M_{m,l}, 0 \le m < K$ and $0 \le l < L$, as shown in Fig. 2. $M_{m,0}$, for example, is computed from (9) as follows:

$$\Pr(s_A^{m,m-1}, s_B^{m,m-1} | s_R^m) \propto \exp\{-\frac{\left\| s_R^m - \frac{1}{K}\sum_i \sum_{l=0}^{1} e^{j\varphi_{i,m}} c_i[l] F_i s_i^{m-l} \right\|^2}{\sigma^2}\}. \quad (10)$$

For $m = 0$, s_i^{-1} is not applicable in (10).

Based on the messages $M_{m,l}$ with the same l, a message passing algorithm can be designed to find the APPs of (s_A^n, s_B^n). We omit the details of the message passing algorithm (similar algorithms can be found in [6], [12]), but point out that the APPs of (s_A^n, s_B^n) will converge due to a tree structure of our factor graph, and that the desired APPs of $(u_A^{2n,2n+1}, u_B^{2n,2n+1})$ are readily obtained according to the QPSK mapping rule. These desired APPs are encapsulated in the messages Q_n in Fig. 2.

Channel decoding of Jt-CNC: This uses the messages Q_n to compute the APPs of $(x_A^m, x_B^m) = (x_A[m], x_B[m])$ and decode $x_A^m \oplus x_B^m$ via a RA channel decoder as depicted in the upper part of Fig. 2. This channel decoder is also a factor graph that shows how X_A (X_B) are correlated with U_A (U_B). X_A and X_B are separately encoded, and each is further divided into a group of odd bits and a group of even bits and the two groups are separately encoded. The same encoding process are performed on these groups. Specifically, $\{x_i^{2m}\}$ ($\{x_i^{2m+1}\}$) are firstly repeated for q times and then interleaved to form $\{\tilde{x}_i^{2n}\}$ ($\{\tilde{x}_i^{2n+1}\}$). $\{u_i^{2n}\}$ (and $\{u_i^{2n+1}\}$) are obtained by accumulating $\{\tilde{x}_i^{2n}\}$ (and $\{\tilde{x}_i^{2n+1}\}$) using XOR. With Q_n fed into this decoder, an iterative message passing algorithm can be designed to compute the APPs of (x_A^m, x_B^m). We briefly describe the message passing in each iteration:

- Upward message passing. Messages are updated in the following sequence: messages from the variable nodes $(u_A^{2n,2n+1}, u_B^{2n,2n+1})$ to the accumulators (blue check nodes with sign '+') $\rightarrow$ messages from the accumulators to the variable nodes $(\tilde{x}_A^{2n,2n+1}, \tilde{x}_B^{2n,2n+1})$ $\rightarrow$ messages from $(\tilde{x}_A^{2n,2n+1}, \tilde{x}_B^{2n,2n+1})$ to the repetition check nodes with sign '=' $\rightarrow$ messages from repetition check nodes to the variable nodes $(x_A^{2m,2m+1}, x_B^{2m,2m+1})$.
- Downward message passing. This reverses both the message direction and the updating sequence in the upward message passing above.

For simplicity, we do not delve into the updating of each message; reference works can be found in [6], [12]. After a certain number of iterations, the APPs of (x_A^{2m}, x_B^{2m}) and (x_A^{2m+1}, x_B^{2m+1}) can be computed from the messages entering the node $(x_A^{2m,2m+1}, x_B^{2m,2m+1})$. Then, X_R is readily obtained from these APPs.

Signal detection of XOR-CD: XOR-CD uses the same factor graph and message passing algorithm as Jt-CNC to compute the APPs of $u_A^n \oplus u_B^n$. It moves one step further after obtaining the APPs of $(u_A^{2n,2n+1}, u_B^{2n,2n+1})$ in Jt-CNC, that is, it derives the APPs of $u_A^{2n} \oplus u_B^{2n}$ and $u_A^{2n+1} \oplus u_B^{2n+1}$ from the APPs of $(u_A^{2n,2n+1}, u_B^{2n,2n+1})$ and uses them as messages Q_{2n} and Q_{2n+1} to be fed into the channel decoder. This simplifies the channel decoding below, but at the cost of information loss with respect to the decoding of X_R.

Channel decoding of XOR-CD: The factor graph of the channel decoder here is essentially the same as that in Jt-CNC except that the variable nodes from top to bottom are replaced with $(x_A^{2m} \oplus x_B^{2m}, x_A^{2m+1} \oplus x_B^{2m+1})$, $(\tilde{x}_A^{2n} \oplus \tilde{x}_B^{2n}, \tilde{x}_A^{2n+1} \oplus \tilde{x}_B^{2n+1})$, and $(u_A^{2n} \oplus u_B^{2n}, u_A^{2n+1} \oplus u_B^{2n+1})$. With the Q_n given by signal detection above, a message passing algorithm similar to that in Jt-CNC can be designed to derive the APPs of $x_A^{2m} \oplus x_B^{2m}$ and $x_A^{2m+1} \oplus x_B^{2m+1}$ and further decode X_R. The message size in XOR-CD is 4 (each variable node is a two-bits vector) whereas it is 16 in Jt-CNC (each variable node is a four-bits vector). Hene, XOR-CD has lower complexities.

Discussion on network coding schemes: Our XOR decoding performs $x_A^{2m} \oplus x_B^{2m}$ (and $x_A^{2m+1} \oplus x_B^{2m+1}$), i.e., network coding is performed on the odd bits (and even bits) of nodes A and B. For QPSK modulation, [10] introduced another scheme that performed network coding on the odd (and even) bits of node A and the even (and odd) bits of node B, and pointed out that the two schemes should be used for different relative phase offsets between the received constellations of the end nodes. With CFO δ_A and δ_B considered, the relative phase offset changes by an amount of $\frac{2\pi(\delta_A - \delta_B)(K+N_g)}{K}$ from one OFDM symbol to its successive symbol. This shows that OFDM symbols in a (long) packet transmission experience different phase offsets under CFO in general. Therefore, CFO blurs the distinction between the two schemes and no one is preferable in the context of CFO in most situations.

B. CFO Compensation

After obtaining the time-domain samples (e.g., $v_R[m]$ in (2) and (6)), relay R could multiply each with a phase term to realize a simultaneous adjustment of the CFO values δ_A and δ_B. Let us denote by τ the amount of adjustment. [6] studied this CFO compensation for PNC with BPSK modulation and revealed that an optimal choice was to set $\tau^* = \frac{\delta_A + \delta_B}{2}$ to result in the two CFO values opposite to each other, i.e., $\frac{\delta_A - \delta_B}{2}$ and $\frac{\delta_B - \delta_A}{2}$. In this paper, we will study by simulation

the effect of setting different τ on the XOR decoding of PNC with QPSK modulation, and show that the optimal choice of τ is also $\tau^* = \frac{\delta_A+\delta_B}{2}$.

C. Pilot Insertion

Traditionally, pilots are inserted into a packet primarily for channel estimation, and more pilots are usually needed in a more dynamic environment [21]. In fact, pilots play an additional role in OFDM based PNC, that is, it can be used effectively against the adverse effect of CFO. The reason is as follows. Pilots are known symbols and thus their interference on other subcarriers (especially their neighboring subcarriers in our system model) can be removed. An immediate consequence is that the signal detection at those neighboring subcarriers is improved. What is more, this benefit can propagate to other subcarriers when using message passing for signal detection [12]. To study this additional role of pilots in our PNC system, we consider uniform pilot placement with a spacing of S_p subcarriers in one OFDM symbol. We make the following modifications to adapt Jt-CNC and XOR-CD to the pilot scenarios:

1) Removing known interference: For each received sample in (9), we remove/subtract the interference caused by the known pilots from the ICI terms.
2) Revising the message contents of $M_{m,l}$: This applies to pilot subcarriers and those with interference dominated by pilot subcarriers to reflect in $M_{m,l}$ the fact that pilots are known symbols. For example, let us consider the case of $\delta_A > 0$ and $\delta_B > 0$ and assume subcarrier m is a pilot subcarrier. Then, the APPs of $(s_A^{m,m-1}, s_B^{m,m-1})$ in $M_{m,l}$ and $(s_A^{m+1,m}, s_B^{m+1,m})$ in $M_{m+1,l}$ are set 0 for (s_A^m, s_B^m) not equal to pilot symbols.

V. Simulation Study

This section evaluates the effectiveness of the proposed schemes/measures against the CFO effect in OFDM based PNC. We adopt the basic settings in the IEEE 802.11p standard [4] for this study: there is a total of $K = 64$ subcarriers, and the number of CP samples is $N_g = 16$. The repetition times of the RA code is $q = 3$, and after channel coding, the packets from nodes A and B have the same length of 240 bytes, corresponding to a total of $L = 15$ OFDM symbols. The number of iterations in RA decoder is set to 10. For simplicity, we assume nodes A and B have sufficient power budget so that $F_i = 1$ holds in (9). The following three studies assume the flat fading channels in TWRC, and the results under frequency-selective channels are presented in a summary.

A. The Close/Equal CFO Case

This subsection assumes close CFO between nodes A and B (or simply $\delta_A = \delta_B$) and studies how Jt-CNC and XOR-CD respond to different SNR and relative phase offsets $\Delta\theta = \varphi_A - \varphi_B$ ($\varphi_{i,m}$ reduces to φ_i in (9) in flat fading channels).

Fig. 3 shows the BER of XOR decoding of PNC at different SNR levels but with $\Delta\theta = 0$. First, at both low and medium CFO levels, Jt-CNC outperforms XOR-CD as SNR increases.

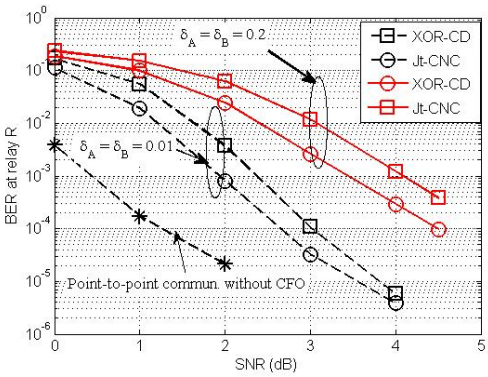

Fig. 3. BER of PNC at different SNR levels with $\delta_A = \delta_B$ and $\Delta\theta = 0$.

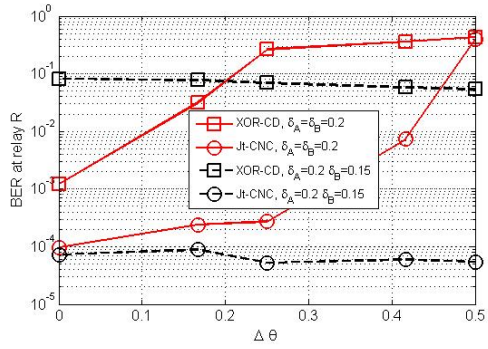

Fig. 4. BER of PNC at different $\Delta\theta$ with fixed SNR = 4 dB.

This is because the XOR operation in the signal detection of XOR-CD induces information loss and degrades the BER. Second, we include point-to-point communications without CFO for comparison. We see from the figure that for a target BER of 10^{-4}, PNC lags 3 to 3.5 dB behind point-to-point communications, but it halves the transmission times.

Fig. 4 shows the BER of PNC at different $\Delta\theta$ for SNR $= 4$ dB. We see that for $\delta_A = \delta_B$, the BER of both Jt-CNC and XOR-CD deteriorate as $\Delta\theta$ increases from 0 to $\frac{\pi}{2}$, whereas they almost stay constant for $\delta_A \neq \delta_B$. This is because in the former case $\Delta\theta$ applies to all OFDM symbols and the adverse effect of a higher $\Delta\theta$ from 0 to $\frac{\pi}{2}$ arises [10], whereas in the latter case, the OFDM symbols in a packet transmission experience different phase offsets regardless of $\Delta\theta$ and hence there is no $\Delta\theta$ that is particularly harmful. Hence, with CFO in PNC, choosing the aforementioned network coding scheme according to $\Delta\theta$ does not make difference and thus either network coding scheme can be used regardless of $\Delta\theta$.

B. Effect of CFO Compensation

We now study the effect of CFO compensation in a TWRC with $\Delta\delta = \delta_A - \delta_B = 0.3$ and SNR $= 4$ dB. The effect of varying the CFO adjustment amount $\tau = \delta_A - \tau'$ is shown in Fig. 5. We see that for both Jt-CNC and XOR-CD the optimal choice of τ is $\tau^* = \frac{\delta_A+\delta_B}{2}$. This is consistent with the optimal τ for BPSK modulation [6]. Moreover, we see from the studies (not shown as figures here) that for a given $|\Delta\delta|$ up to 0.3,

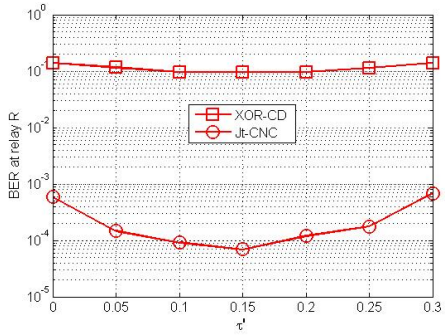

Fig. 5. Effect of CFO compensation on PNC.

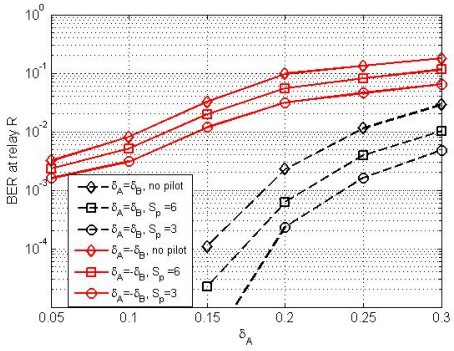

Fig. 6. Effect of pilot insertion on PNC.

with the optimal τ^*, Jt-CNC lags at most 3 dB SNR behind point-to-point communications for a target BER of 10^{-4}.

C. Effect of Pilot Insertion

Here we study the effect of pilot insertion in the following two cases: (1) $\delta_A = \delta_B$ and $\Delta\delta = 0$ and (2) $\delta_A = -\delta_B$ (resulting from the optimal CFO compensation). To see the effect clearly, we set a high SNR level, $= 20$ dB, and look at the BER of signal detection (of XOR-CD here) in PNC. Fig. 6 shows the BER of PNC varies with δ_A and pilot spacing S_p, where we see a positive effect of inserting more pilots (i.e., a lower S_p) in both cases. However, using more pilots sacrifices data subcarriers. We leave the study of an optimal number of pilots for PNC under CFO as future work.

For PNC under frequency-selective channels with $F_i = 1$, we have conducted simulation (not shows as figures due to page limit) and observed that (1) the XOR decoding is improved with more pilots, and (2) the optimal CFO compensation also applies, and with it, both Jt-CNC and XOR-CD perform nearly the same as in flat fading channels.

VI. Conclusion

This paper dealt with the carrier frequency offset problem in OFDM based PNC with QPSK modulation. It firstly put forth two signal detection and decoding schemes for the XOR decoding of PNC. It also studied the effect of CFO compensation and pointed out an optimal CFO compensation that was optimal for PNC with both BPSK and QPSK modulations. Moreover, it used pilots against the CFO effect and such enhancement was demonstrated in our preliminary studies. With all the proposed measures, it was revealed that for low to medium CFO level, the BER of PNC is comparable to that of point-to-point communications, but it halves the transmission times. Our future study is to further investigate pilot insertion by incorporating channel estimation in PNC.

References

[1] L. Dai, *et al.*, "A survey of non-orthogonal multiple access for 5G," *IEEE COMMUNICATIONS SURVEYS and TUTORIALS*, vol. 20, no. 3, pp. 2294 - 2323, 2018.

[2] S. Zhang, S. C. Liew, and P. P. Lam, "Physical-layer network coding," in *Proc. of MobiCom*, 2006.

[3] Z. Situ, I. W.-H. Ho, T. Wang, S. C. Liew, C.-K. Chau, "OFDM Modulated PNC in V2X Communications: An ICI-aware Approach against CFOs and Time-frequency-selective Channels," *IEEE Access*, vol. 7, no. 1, pp. 4880 C 4897, 2019.

[4] L. F. Xie, I. W. H. Ho, S. C. Liew, L. Lu, and F. C. M. Lau, "The feasibility of mobile physical-layer network coding with BPSK modulation," *IEEE Trans. Vehicular Technology*, vol. 66, no. 5, 2017.

[5] Z. Wang, J. Huang, S. Zhou, and Z. Wang, "Iterative receiver processing for OFDM modulated physical-layer network coding in underwater acoustic channels," *IEEE Trans. Commun.*, vol. 61, no. 2, pp. 541 - 553, 2013.

[6] L. F. Xie, *et al.*, "Channel-Coded Physical-Layer Network Coding With OFDM Modulation," *IEEE Access*, vol. 6, 2018.

[7] S. Zhang, S. C. Liew, and H. Wang, "Synchronization analysis for wireless TWRC operated with physical-layer network coding," *Wireless Personal Communications*, Springer, vol. 68, no. 3, pp. 647-653, 2013.

[8] Y. Shao, S. C. Liew, and L. Lu, "Asynchronous physical-layer network coding: symbol misalignment estimation and its effect on decoding," *IEEE Trans. Wireless Commun.*, vol. 16, no. 10, 2017.

[9] L. Lu, T. Wang, S. C. Liew, and S. Zhang, "Implementation of physical-layer network coding," *Physical Communication*, vol. 6, 2013.

[10] T. Koike-Akino, P. Popovski, and V. Tarokh, "Optimized constellations for two-way wireless relaying with physical network coding," *IEEE J. Sel. Areas Commun.*, vol. 27, no. 5, pp. 773 - 787, 2009.

[11] Y. Huang, S. Wang, Q. Song, L. Guo, and A. Jamalipour, "Synchronous physical-layer network coding: a feasibility study," *IEEE Trans. Wireless Commun.*, vol. 12, no. 8, pp. 4048 - 4057, 2013.

[12] L. Lu, and S. C. Liew, "Asynchronous physical-layer network coding," *IEEE Trans. Wireless Commun.*, vol. 11, no. 2, pp. 819 - 831, 2012.

[13] M. Woltering, D. Wubben, and A. Dekorsy, "Physical layer network coding with Gaussian waveforms using soft interference cancellation," in *Proc. of VTC Spring*, 2015.

[14] L. Lu, L. You, and S. C. Liew, "Network-coded multiple access," *IEEE Trans. Mobile Computing*, vol. 13, no. 12, pp.2853 - 2869, 2014.

[15] L. You, S. C. Liew, and L. Lu, "Network-coded multiple access II: toward real-time operation with improved performance," *IEEE J. Sel. Areas Commun.*, vol. 33, no. 2, pp. 264 - 280, 2015.

[16] T. Wang and S. C. Liew, "Joint channel estimation and channel decoding in physical-layer network coding systems: an EM-BP factor graph framework," *IEEE Trans. Wireless Commun.*, vol. 13, no. 4, 2014.

[17] S. Brink and G. Kramer, "Design of repeat-accumulate codes for iterative detection and decoding," *IEEE Trans. Signal Process.*, vol. 5, no. 11, pp. 2764 - 2772, 2003.

[18] G. Bartoli, R. Fantacci, D. Marabissi, and R. Simoni, "Subcarrier suppression methods for OFDM systems with decode-and-forward network coding," *IEEE Trans. Wireless Commun.*, vol. 12, no. 12, pp. 6034 - 6042, 2013.

[19] M. Stojanovic, "Low complexity OFDM detector for underwater acoustic channels," in *Proc. of IEEE OCEANS*, 2006.

[20] A. Salberg and A. Swami, "Doppler and Frequency-Offset Synchronization in Wideband OFDM," *IEEE Trans. Wireless Commun.*, vol. 4, no. 6, 2005.

[21] K. K. Nagalapur, *et al.*, "An 802.11p cross-layered pilot scheme for time- and frequency-varying channels and its hardware implementation," *IEEE Trans. Vehicular Technology*, vol. 65, no. 6, pp. 3917 - 3928, 2016.